Journal of Geophysical Research: Biogeosciences

RESEARCH ARTICLE
10.1029/2018JG004482

Disentangling Climate and LAI Effects on Seasonal Variability in Water Use Efficiency Across Terrestrial Ecosystems in China

Yue Li[1,2], Hao Shi[3], Lei Zhou[4], Derek Eamus[5,6], Alfredo Huete[5], Longhui Li[5], James Cleverly[5,6], Zhongmin Hu[7], Mahrita Harahap[5], Qiang Yu[3,5], Liang He[8], and Shaoqiang Wang[1,2]

[1]Key Laboratory of Ecosystem Network Observation and Modeling, Institute of Geographic Sciences and Natural Resources Research, Chinese Academy of Sciences, Beijing, China, [2]College of Resources and Environment, University of Chinese Academy of Sciences, Beijing, China, [3]State Key Laboratory of Soil Erosion and Dryland Farming on the Loess Plateau, Northwest A & F University, Yangling, China, [4]College of Geography and Environmental Sciences, Zhejiang Normal University, Jinhua, China, [5]School of Life Sciences, University of Technology Sydney, Sydney, New South Wales, Australia, [6]Australian Supersite Network, Terrestrial Ecosystem Research Network, University of Technology Sydney, Sydney, New South Wales, Australia, [7]School of Geography, South China Normal University, Guangzhou, China, [8]Agro-meteorological Center, National Meteorological Center of China Meteorological Administration, Beijing, China

Key Points:
- A new algorithm based on partial least squares regression was developed to discern the individual effects of multiple variables on WUE
- Leaf area index played an important role in influencing seasonal variability in WUE compared to climatic variables
- The algorithm can inform the design of field experiments and factorial simulations to discern key drivers for ecosystem functions

Correspondence to:
H. Shi and S. Wang,
yuren2006@gmail.com;
sqwang@igsnrr.ac.cn

Citation:
Li, Y., Shi, H., Zhou, L., Eamus, D., Huete, A., Li, L., et al. (2018). Disentangling climate and LAI effects on seasonal variability in water use efficiency across terrestrial ecosystems in China. *Journal of Geophysical Research: Biogeosciences*, *123*, 2429–2443. https://doi.org/10.1029/2018JG004482

Received 9 MAR 2018
Accepted 24 JUL 2018
Accepted article online 2 AUG 2018
Published online 20 AUG 2018

Abstract Water use efficiency (WUE), the ratio of gross primary productivity (GPP) over evapotranspiration (ET), is a critical ecosystem function. However, it is difficult to distinguish the individual effects of climatic variables and leaf area index (LAI) on WUE, mainly due to the high collinearity among these factors. Here we proposed a partial least squares regression-based sensitivity algorithm to confront the issue, which was first verified at seven ChinaFlux sites and then applied across China. The results showed that across all biomes in China, monthly GPP (0.42–0.65), ET (0.33–0.56), and WUE (0.01–0.31) showed positive sensitivities to air temperature, particularly in croplands in northeast China and forests in southwest China. Radiation exerted stronger effects on ET (0.55–0.78) than GPP (0.19–0.65), resulting in negative responses (−0.44 to 0.04) of WUE to increased radiation among most biomes. Increasing precipitation stimulated both GPP (0.06–0.17) and ET (0.05–0.12) at the biome level, but spatially negative effects of excessive precipitation were also found in some grasslands. Both monthly GPP (−0.01 to 0.29) and ET (0.02–0.12) showed weak or moderate responses to vapor pressure deficit among biomes, resulting in weak response of monthly WUE to vapor pressure deficit (−0.04 to 0.08). LAI showed positive effects on GPP (0.18–0.60), ET (0–0.23), and WUE (0.13–0.42) across biomes, particularly on WUE in grasslands (0.42 ± 0.30). Our results highlighted the importance of LAI in influencing WUE against climatic variables. Furthermore, the sensitivity algorithm can be used to inform the design of manipulative experiments and compare with factorial simulations for discerning effects of various variables on ecosystem functions.

1. Introduction

Vegetation assimilates CO_2 from the atmosphere through photosynthesis, accompanied by the loss of water via transpiration. The ratio of assimilation (i.e., gross primary productivity, GPP) to total ecosystem water loss (i.e., evapotranspiration, ET), defined as ecosystem water use efficiency (WUE), reflects the trade-off between carbon and water exchange (Law et al., 2002; Zhou et al., 2015). WUE integrates a suite of biotic and climatic factors (Keenan et al., 2013) and is thus an excellent indicator of ecosystem responses to climate variability (Campos et al., 2013), vegetation dynamics, and human activities (F. M. Zhang et al., 2013).

The behavior of WUE among different biomes has been extensively studied using multiple approaches over various spatiotemporal scales, such as manipulative experiments (Niu et al., 2011; Quan et al., 2018), eddy covariance observations (Law et al., 2002; Ponton et al., 2006; Shi et al., 2014), isotope techniques (Ponton et al., 2006), and process-based models (Huang et al., 2015; F. M. Zhang et al., 2013). However, studies on WUE responses to the same climatic or biotic factors are often inconsistent and even contrary in some cases (Ainsworth & Rogers, 2007; Keenan et al., 2013; Li et al., 2008; Mastrotheodoros et al., 2017). For example, Bai et al. (2008) reported that ecosystem WUE increased with increasing annual precipitation (Prcp), while Li et al. (2008) obtained an opposite result. For another example, WUE is usually expected to decrease with increasing

vapor pressure deficit (VPD, Law et al., 2002) across various time scales. However, in some cases such a response of WUE to VPD might only exist seasonally (Eamus, Boulain, et al., 2013) or even does not exist at all due to droughts (Reichstein et al., 2002). In addition, WUE has also been found to be strongly correlated with air temperature (T_a), radiation (Rad), soil water content (SWC) and leaf area index (LAI, Hu et al., 2008; Li et al., 2008; Yu et al., 2008; F. M. Zhang et al., 2013). These phenomena reflect the complexity in distinguishing the major driving variable for WUE variations, presumably due to the differential responses of GPP and ET to environmental and biotic factors (Brümmer et al., 2012). Therefore, it is critical to clarify the individual responses of GPP and ET and the effects of single variables to determine how WUE changes in a changing environment.

Factorial experiments in the field are ideal for discerning the independent effects of climatic and biotic variables. However, most such experiments have been conducted at the plot or plant level and thus have limited treatments due to financial and time constraints. It is difficult to translate local-scale results to the ecosystem scale (Norby & Zak, 2011), especially if the response of GPP and ET to abiotic and biotic variables varies across spatial and temporal scales (Lindroth & Cienciala, 1996). Furthermore, limited numbers of treatments may be insufficient to clarify interactions among multiple environmental variables (Norby & Luo, 2004). Although running factorial simulations by process-based models is plausible, it is difficult to validate the results of these simulations at plot and regional scales. Therefore, a statistical evaluation of the response of WUE to environmental changes at the ecosystem scale is critically needed. The advantage of statistical disaggregation of the effects of single variables in driving WUE is that it allows some ground truth through comparison with ecosystem-level observations such as eddy covariance measurements.

The simple (SLR) or multiple (MLR) linear regression model is often used to account for the response of one dependent variable to multiple predictor variables. However, the results by MLR can become problematic if there is high collinearity among predictor variables, which often occurs to ecological data (Graham, 2003). Specifically, MLR can significantly bias relationships between the dependent variable and the predictor variables in the presence of even minor collinearity and inflate the standard errors of the estimated regression coefficients, leading individual predictor variables to look insignificant (Graham, 2003).

To address the above issue, we developed a new algorithm that calculates the actual sensitivities of GPP, ET, and WUE (the dependent variables) as a product of their apparent sensitivities (the ratio of change in a dependent variable over the change in a predictor variable) to environmental drivers (the predictor variables) with the corresponding weights of each predictor variable. The weights of predictor variables are computed based on the partial least squares regression (PLSR) method, which can effectively reduce uncertainties induced by high collinearity among predictor variables. We applied the algorithm to calculate the sensitivities of monthly GPP, ET, and WUE to climate variables and LAI at seven ChinaFlux (Chinese Terrestrial Ecosystem Flux Observational Network) sites. These sites cover a range of vegetation and climate types. We then compared this algorithm with the conventional MLR model. Finally, the verified algorithm was applied to the whole of China to investigate how GPP, ET, and WUE might respond to seasonal climate and LAI variability among biomes using monthly data-driven GPP/ET products, meteorological data, and satellite retrievals of LAI from 1982 to 2010.

2. Materials and Methods

2.1. Flux Sites

Seven sites (Figure 1 and Table 1) from ChinaFLUX with contrasting climate regimes (Figure 1) were selected to examine the sensitivities of WUE to monthly climate variability and LAI. These sites cover several ecosystem types, including crops (CRO, one site), deciduous broadleaf forest (DBF, one site), evergreen broadleaf forest (EBF, two sites), evergreen needle-leaved forest (ENF, one site), and grasslands (GRA, two sites). The Yucheng site (CN-Yuc) is a warm temperate dry farming cropland located in the North China Plain (Yu et al., 2006) with a crop rotation of winter wheat and summer maize. The Changbaishan site (CN-Cha) located in Northeast China is a DBF ecosystem, dominated by 200-year old Korean pine (*Pinus koraiensis*) and dense understory shrubs (J. H. Zhang et al., 2009). The two EBF sites, Dinghushan (CN-Din) and Xishuangbanna (CN-Xsh), have contrasting climate conditions and vegetation. CN-Din is in a subtropical climate and is dominated by *Schima superb* and *Castanopsis chinensi* (Yu et al., 2008), whereas the CN-Xsh site is a tropical rainforest with distinct wet and dry seasons (Tan et al., 2013). The Qianyanzhou site (CN-Qia) is the only ENF

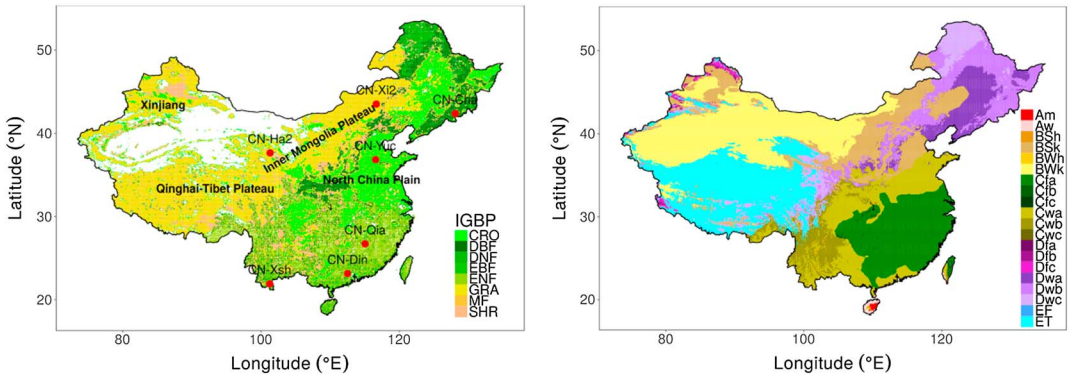

Figure 1. The left panel shows locations of the seven ChinaFlux sites used in this study. The background is the spatial distribution of land cover across China in 2010. Terrestrial ecosystems in China are grouped into CRO = crops; DBF = deciduous broadleaf forest; DNF = deciduous needle-leaved forest; EBF evergreen broadleaf forest; ENF = evergreen needle-leaved forest; GRA = grasslands; MF = mixed forests; and SHR = shrublands. The right panel shows the Köppen-Geiger climate classification in China. Main climates: A = equatorial; B = arid; C = warm temperate; D = snow; and E = polar; precipitation: W = desert; S = steppe; f = fully humid; w = winter dry; and m = monsoonal; temperature: h = hot arid; k = cold arid; a = hot summer; b = warm summer; c = cool summer; F = polar frost; and T = polar tundra.

ecosystem with a subtropical monsoon climate. The dominant species are Slash pine (*Pinus elliottii*), Masson pine (*Pinus massoniana*), and Chinese fir (*Cunninghamia lanceolata*) planted around 1985. Two grassland sites are included: the water-limited Xilinhot temperate steppe (CN-Xi2) in Inner Mongolia and the low-temperature Haibei alpine meadow (CN-Ha2) in the Qinghai-Tibet Plateau. The dominant species are *Leymus chinensis*, *Stipa grandis*, and *Agropyron cristatum* at CN-Xi2 and *Potentilla fruticosa*, *Kobresia capillifolia*, and *Kobresia humilis* at CN-Ha2 (Guo et al., 2015).

Half-hourly eddy covariance measurements of carbon, water, and energy fluxes and auxiliary observations of meteorological and soil variables were collected during 2003–2010 at the seven sites and processed following the standard ChinaFLUX quality control and gap-filling routines (Yu et al., 2006). GPP was calculated as the sum of daily net ecosystem carbon exchange and daily ecosystem respiration, with the latter derived from the relationship between nocturnal net ecosystem carbon exchange and soil temperature and SWC. In addition, we extracted concurrent LAI data from the 8-day MOD15A2 product (1-km resolution) using a central 3 × 3-km window around each of the flux towers. Only LAI pixels with cloud state values less than 2 and confidence score values less than 3 were used to calculate the average. All data were then aggregated into a monthly time step.

2.2. Spatial Data Sets

At the country scale, monthly GPP and ET products (Jung et al., 2009, 2011) with a 0.5° × 0.5° resolution were used to calculate monthly WUE from 1982 to 2010. These products are upscaled from FLUXNET (https://

Table 1
Descriptions for the Seven Sites Used in This Study

ID	Biome	Lat (°N)	Lon (°E)	MAT (°C)	MAP(mm/year)	ET(mm/year)	GPP(g C·m^{-2}·year^{-1})	WUE(g C/kg H_2O)	Growing season	Period
CN-Yuc	CRO	36.83	116.57	13.3	617.3	545.1	2206.1	4.1	Feb–Nov	2003–2010
CN-Cha	DBF	42.40	128.10	3.6	472.2	398.5	1590.3	4.0	Apr–Oct	2003–2010
CN-Din	EBF	23.17	112.52	20.1	1477.9	641.9	1484.7	2.3	Jan–Dec	2003–2010
CN-Xsh	EBF	21.93	101.27	19.4	1237.6	637.2	2253.8	3.5	Jan–Dec	2003–2010
CN-Qia	ENF	26.74	115.06	17.7	1197.3	676.2	1810.0	2.7	Jan–Dec	2003–2010
CN-Ha2	GRA	37.67	101.33	−1.4	513.1	531.3	956.3	1.8	May–Sep	2003–2010
CN-Xi2	GRA	43.53	116.67	1.5	234.7	229.2	400.6	1.8	Apr–Oct	2003–2010

Note. Descriptions include site name (ID), latitude (Lat, °N), longitude (Lon, °E), mean annual temperature (MAT, °C), mean annual precipitation (MAP, mm/year), biome classification, mean annual GPP (g C·m^{-2}·year^{-1}), mean annual growing season ET (mm/year), mean annual growing season WUE (g C/kg H_2O), growing season months of the year, and measurement periods. GPP = gross primary productivity; ET = evapotranspiration; WUE = water use efficiency; CRO = crops; DBF = deciduous broadleaf forest; EBF = evergreen broadleaf forest; ENF = evergreen needle-leaved forest; GRA = grasslands.

fluxnet.ornl.gov/) measurements using the model tree ensemble (MTE) method. The MTE products integrate information from satellite measurements of vegetation characteristics and gridded climate data but do not consider physiological effects of increasing atmospheric CO_2 concentration and nitrogen deposition. This deficit prevents MTE products from being used in long-term WUE trend analysis (Huang et al., 2016) but has only a minor influence on the analysis of variability in WUE (Huang et al., 2015). The monthly climate data (CRU-NCEP v8.0, https://vesg.ipsl.upmc.fr/thredds/catalog/work/p529viov/cruncep/V8_1901_2016/catalog.html), including air temperature, shortwave radiation, precipitation, and VPD, were a fusion of products by the Climate Research Unit (CRU) and the National Center for Environmental Prediction (NCEP)/National Center for Atmospheric Research (NCAR) with a spatial resolution of 0.5° × 0.5° (Wei et al., 2014). The GLOBMAP LAI (Liu et al., 2012) data, constructed by fusing Advanced Very High Resolution Radiometer (AVHRR) LAI (1981–2000) and Moderate Resolution Imaging Spectroradiometer (MODIS) LAI (2000–2011), were used to indicate the vegetation states. The temporal resolution of GLOBMAP LAI is half monthly, with a spatial resolution of 8 km. The land cover map was derived from the merging of Landsat TM/ETM and HJ-1 satellite retrievals in 2010 with a spatial resolution of 250 m (Wu et al., 2014). In addition, to compare with the MTE ET data, the MOD16A2 ET product (at a monthly step and a spatial resolution of 0.05°) during 2000–2010 was also used. All data were aggregated into a monthly time step and a spatial resolution of 0.5° × 0.5°.

2.3. Disentangling Algorithm

A typical SLR or MLR for one dependent variable with n samples and m independent variables can be represented in the matrix form as

$$\mathbf{y}=\mathbf{Xb}+\mathbf{e} \tag{1}$$

where $\boldsymbol{y}$ is a column vector (n samples) of the dependent variable, $\boldsymbol{X}$ is a $m \times n$ matrix of independent variables, and $\boldsymbol{e}$ denotes a column vector (n samples) of the residual errors. The unknown $\boldsymbol{b}$ can be calculated through minimizing the sum of squared residual errors ($\boldsymbol{e}^T\boldsymbol{e}$). However, such a solution can become invalid or ill conditioned, while $\boldsymbol{X}^T\boldsymbol{X}$ is singular due to collinearity between independent variables (Mevik & Wehrens, 2007).

To circumvent the above deficit of SLR and MLR, the PLSR method is developed. The basic principle of PLSR is to reduce redundant information by projecting $\boldsymbol{X}$ into a lower-dimensional space constituted by so-called principal components (PCs) and then regress $\boldsymbol{y}$ on PCs. The first step is to standardize all dependent and independent variables following

$$y_i = \frac{y_i - \overline{y}}{\sigma_y} \tag{2}$$

where y_i is the ith member of dependent variable $\boldsymbol{y}$, $\overline{y}$ is the average of $\boldsymbol{y}$, and σ_y is the standard deviation of $\boldsymbol{y}$.

The second step is to decompose $\boldsymbol{X}$ into orthogonal PCs. Instead of using the usual singular value decomposition (SVD) method to $\boldsymbol{X}$ to generate PCs, which only considers the substructure information about $\boldsymbol{X}$ when extracting PCs (Mevik & Wehrens, 2007), PLSR uses a *deflation* method to obtain PCs iteratively. It starts with the SVD of the matrix $\boldsymbol{X}^T\boldsymbol{y}$, and the first left and right singular vectors, $\boldsymbol{w}$ and $\boldsymbol{q}$, are then used to weigh $\boldsymbol{X}$ and $\boldsymbol{y}$, respectively, to obtain scores $\boldsymbol{t}$ and $\boldsymbol{u}$ for the first PCs of $\boldsymbol{X}$ and $\boldsymbol{y}$:

$$\begin{aligned}\boldsymbol{t}&=\boldsymbol{Xw}\\ \boldsymbol{u}&=\boldsymbol{yq}.\end{aligned} \tag{3}$$

The loadings for the first PCs of $\boldsymbol{X}$ and $\boldsymbol{y}$, $\boldsymbol{p}$ and $\boldsymbol{q}$, are then calculated as

$$\begin{aligned}\boldsymbol{p}&=\boldsymbol{X}^T\boldsymbol{t}\\ \boldsymbol{q}&=\boldsymbol{y}^T\boldsymbol{t}.\end{aligned} \tag{4}$$

Next, $\boldsymbol{X}$ and $\boldsymbol{y}$ are deflated by subtracting the outer products $\boldsymbol{tp}^T$ and $\boldsymbol{tq}^T$:

$$\begin{aligned} \boldsymbol{X}_{n+1} &= \boldsymbol{X}_n - \boldsymbol{t}\boldsymbol{p}^T \\ \boldsymbol{y}_{n+1} &= \boldsymbol{y}_n - \boldsymbol{t}\boldsymbol{q}^T. \end{aligned} \tag{5}$$

The next PC then can start from the SVD of $\boldsymbol{X}_{n+1}^T\boldsymbol{y}_{n+1}$ until the number of PCs reaches the optimum. Vectors $\boldsymbol{w}$, $\boldsymbol{t}$, and $\boldsymbol{p}$ in each iteration constitute matrices $\boldsymbol{W}$, $\boldsymbol{T}$, and $\boldsymbol{P}$.

The third step is to regress $\boldsymbol{y}$ against PC scores to obtain regression slopes as

$$\mathbf{b} = \mathbf{R}\left(\mathbf{T}^{\mathbf{T}}\mathbf{T}\right)^{-1}\mathbf{T}^{\mathbf{T}}\mathbf{y} \tag{6}$$

where $\boldsymbol{b}$ is a column vector of m elements, and $\boldsymbol{R} = \boldsymbol{W}(\boldsymbol{P}^T\boldsymbol{W})^{-1}$ indicates the inflated loadings by the weight matrix $\boldsymbol{W}$. Simultaneously, accompanying $\boldsymbol{b}$, we can get a significance vector, which is then used to select significant $\boldsymbol{b}$ and PC loadings at a significant level of 0.05. For these significant $\boldsymbol{b}$ values, we multiplied the $\boldsymbol{b}$ values and corresponding PC loadings for each variable in $\boldsymbol{X}$ and then sum these products as

$$\mathbf{w_i} = \sum_{\mathbf{j}=1}^{\mathbf{k}} \mathbf{b_j}\mathbf{R_{i,j}} \tag{7}$$

where b_j is the slope for the jth significant PC, $R_{i,j}$ is the jth significant PC loading for the ith variable in $\boldsymbol{X}$, k is the number of significant PCs, and w_i indicates the relative importance of the ith variable in explaining the variance of $\boldsymbol{y}$. w_i is then used to weigh the apparent sensitivity of $\boldsymbol{y}$ to each variable X_i in $\boldsymbol{X}$, which was calculated following (Raupach et al., 2013) as

$$a_{X_i}^y = \frac{\sigma_y}{\overline{y}} \Big/ \frac{\sigma_{X_i}}{\overline{X_i}} \tag{8}$$

where σ_y is the standard deviation of $\boldsymbol{y}$, $\overline{y}$ is the mean value of $\boldsymbol{y}$, and $a_{X_i}^y$ indicates the apparent sensitivity of $\boldsymbol{y}$ to the ith variable in $\boldsymbol{X}$. The benefit of the $a_{X_i}^y$ definition is that sensitivities of different dependent variables to different independent variables can be directly compared to each other. Further, we obtained the weighted sensitivity of $\boldsymbol{y}$ to the ith variable in $\boldsymbol{X}$ as

$$s_{x_i}^y = w_i a_{X_i}^y \tag{9}$$

2.4. Application of the New Algorithm to Sites and the Whole Country

Specifically, we selected monthly air temperature, solar radiation, precipitation, VPD, and LAI as independent variables in both site- and country-scale analyses. The growing season period for each site or grid cell was defined following (1) the multiyear mean monthly temperature should be larger than 0 °C, and (2) the multiyear mean monthly GPP should be larger than 10 g C·m^{-2}·month^{-1}. Besides computing WUE sensitivity ($s_{C\,\mathrm{lim/LAI}}^{\mathrm{WUE}}$) directly, we also partitioned variability in WUE into its two contributive components: GPP and ET. Theoretically, the relative change between sensitivities of GPP ($s_{C\,\mathrm{lim/LAI}}^{\mathrm{GPP}}$) and ET ($s_{C\,\mathrm{lim/LAI}}^{\mathrm{ET}}$) can explain the response of WUE to climate and LAI variability (derived $s_{C\,\mathrm{lim/LAI}}^{\mathrm{WUE}} \approx \left(1 + s_{C\,\mathrm{lim/LAI}}^{\mathrm{GPP}}\right) / \left(1 + s_{C\,\mathrm{lim/LAI}}^{\mathrm{ET}}\right) - 1$), and this relative change can be used to verify whether the sensitivity algorithm is robust. However, due to the data uncertainties, the derived $s_{C\,\mathrm{lim/LAI}}^{\mathrm{WUE}}$ could be different from the directly computed $s_{C\,\mathrm{lim/LAI}}^{\mathrm{WUE}}$ due to biased $s_{C\,\mathrm{lim/LAI}}^{\mathrm{GPP}}$ and $s_{C\,\mathrm{lim/LAI}}^{\mathrm{ET}}$. To alleviate the influence of too short a period of observations, we conducted the sensitivity analysis nine times at the site level by removing in each iteration 0 or 1 year of data from the total 8-year observations. Thus, there were nine sensitivity values estimated for GPP, ET, or WUE in response to each predictor variable. To compare the PLSR-based algorithm with the MLR model, the same strategy was used in the MLR analysis. At the country level, no extra sensitivity analysis was conducted because the data length of nearly three decades was enough to reduce uncertainty.

3. Results

3.1. Site-Level Sensitivity Analysis

Among all sites, GPP tended to show positive sensitivities to air temperature, radiation, precipitation, and LAI but negative sensitivity to VPD during the observation periods (Figure 2a). In the MLR analysis, the significant

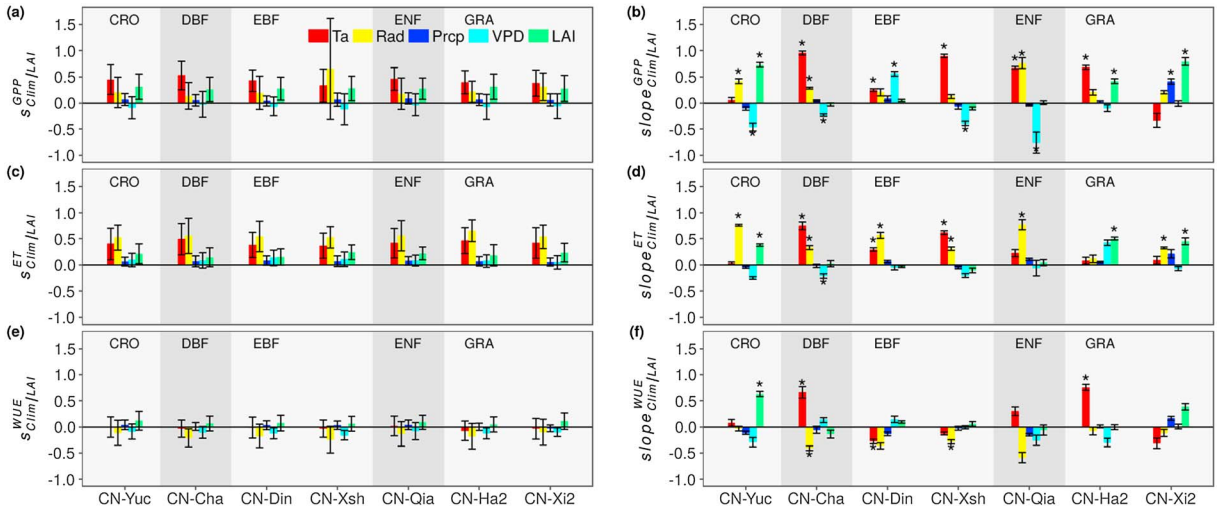

Figure 2. Comparison of the partial least squares regression-based (a, c, e) and multiple linear regression-based (b, d, f) sensitivities of GPP, ET, and WUE to monthly variability in climate and LAI during 2003–2010. Sensitivities of each dependent variable to each predictor variable are calculated nine times at every site, and the bars indicate the standard deviation. The "*" symbol indicates that there are at least seven significant ($p < 0.05$) estimates of sensitivities of a dependent variable to a particular predictor variable, and the mean value and the standard deviation are calculated from only the significant estimates. Otherwise, the mean value and the standard deviation are calculated from all the estimates by the nine times of calculation. The shades are to annotate neighboring biomes. GPP = gross primary productivity; ET = evapotranspiration; WUE = water use efficiency; LAI = leaf area index; VPD = vapor pressure deficit; CRO = crops; DBF = deciduous broadleaf forest; EBF = evergreen broadleaf forest; ENF = evergreen needle-leaved forest; GRA = grasslands.

estimates of GPP responses to LAI and climatic variables were consistent with those estimated by the PLSR-based algorithm in most cases (Figure 2b). However, it is noted that the MLR model estimated a strong positive effect of VPD on GPP at one EBF site (CN-Din) in contrast to a relatively low sensitivity of GPP to VPD by PLSR. Furthermore, the MLR model failed to give significant ($p < 0.05$) estimates on GPP sensitivities to climatic variables or LAI in all the nine times of calculation (Figure 2b). For example, at the temperature-dominated alpine meadow (CN-Ha2), precipitation showed no significant effect on GPP in at least one time of calculation, which was against the previous study by Guo et al. (2015).

Across all sites, the PLSR-based algorithm estimated that ET was most sensitive to radiation, air temperature, and LAI in order (Figure 2c). In contrast, the MLR model could only give significant estimates for effects of part of variables at a specific site (Figure 2d). But the significant estimates by the MLR model were basically positive consistent with those by the PLSR-based algorithm, except that the MLR model estimated a significant negative effect of VPD on ET at the DBF site (CN-Cha).

The effects of climatic and LAI variables on WUE depended on their separate effects on GPP and ET. In most cases, both the PLSR-based algorithm and the MLR model predicted reasonable WUE changes given the relative responses of GPP and ET to the same environmental variable according to the derived sensitivity equation (Figure 2). For example, at the CN-Cha site, $s^{GPP}_{C\,lim/LAI} = 0.26 \pm 0.23$ and $s^{ET}_{C\,lim/LAI} = 0.15 \pm 0.18$. The derived $s^{WUE}_{C\,lim/LAI} = 0.096$, while the directly computed $s^{WUE}_{C\,lim/LAI} = 0.07 \pm 0.14$. However, in some cases, the MLR method failed to explain the WUE response. For example, at one of the subtropical EBF sites (CN-Xsh), although temperature showed larger significant influence on the monthly variability of GPP than that on ET, the MLR model obtained a negative effect of temperature on WUE (Figure 2).

3.2. Country-Level Sensitivity Analysis

Figure 3a shows the spatial distribution of the predictor variables to which the monthly variability of GPP was the most sensitive in each grid cell. GPP was the most sensitive to temperature in crops in northeastern China and radiation in northern forests and Xinjiang grasslands, while GPP was the most sensitive to LAI or temperature in grasslands along the Inner Mongolia Plateau and radiation or VPD in the Qinghai-Tibet Plateau. Across the whole country, increasing air temperature could stimulate GPP across the majority of China, particularly in northern and southwestern China (Figure 3b). Increased radiation could benefit GPP in southeast and the majority of northeast China and North China Plain. Negative effects of increased radiation were mainly found in semiarid and arid grasslands, including parts of the Inner Mongolia Plateau and particularly the Qinghai-

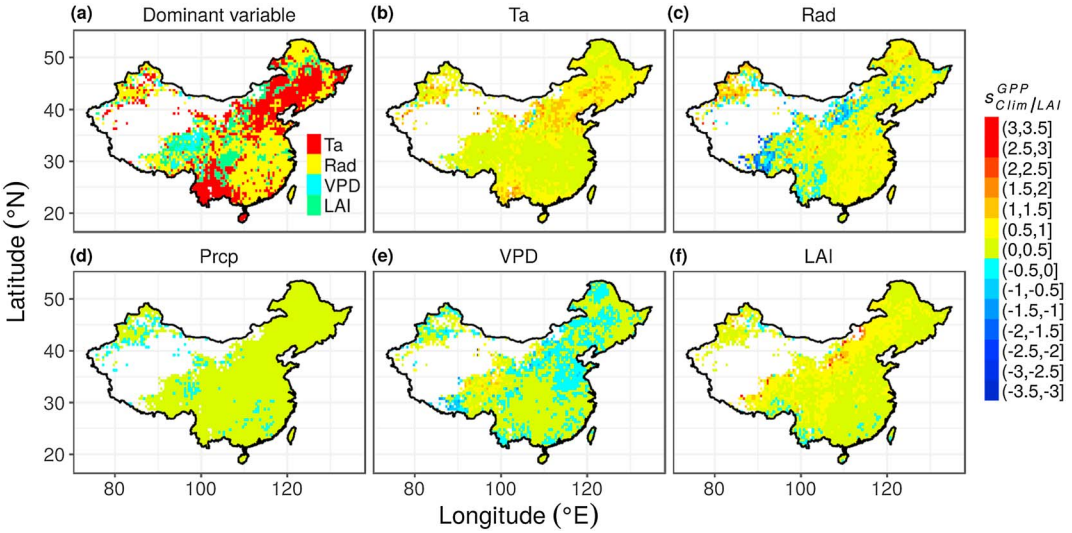

Figure 3. Spatial distribution of (a) variables (climate or LAI) to which GPP is most sensitive and the sensitivities of GPP to monthly variability in (b) air temperature (T_a), (c) solar radiation (Rad), (d) precipitation (Prcp), (e) VPD, and (f) LAI during 1982–2010. Panel a uses its own categorical legend, while all the other panels share the continuous legend in the right of the figure. LAI = leaf area index; GPP = gross primary productivity; VPD = vapor pressure deficit.

Tibet Plateau, and the eastern edge of the alpine regions of northern Xinjiang (Figure 3c). Weak to moderate negative effects of precipitation on GPP were found in parts of the Xinjiang alpine meadows and grasslands in the northern Qinghai-Tibet Plateau (Figure 3d). In contrast, GPP was positively sensitive to precipitation in most grasslands, crops, and forests (Figure 3d). VPD showed negative effects on GPP mainly in northern China but weak to moderate positive effects in the majority of south China and the Qinghai-Tibet Plateau (Figure 3e). LAI showed positive effects on GPP in majority of the country, particularly in the grasslands of the Inner Mongolia Plateau and Qinghai-Tibet Plateau (Figure 3f).

The spatial patterns of ET sensitivities to climatic and LAI variables showed some similarity to those of sensitivities of GPP suggesting the tight coupling of GPP and ET (Figures 3 and 4). However, the patterns of ET

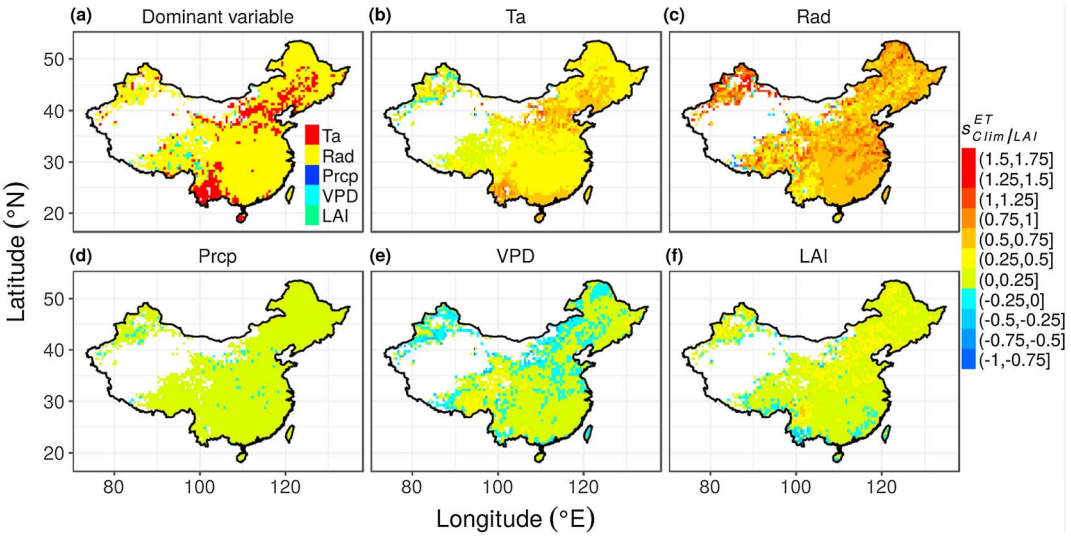

Figure 4. Spatial distribution of (a) variables (climate or LAI) to which ET is most sensitive and the sensitivities of ET to monthly variability in (b) air temperature (T_a), (c) solar radiation (Rad), (d) precipitation (Prcp), (e) VPD, and (f) LAI during 1982–2010. Panel a uses its own categorical legend, while all the other panels share the continuous legend in the right of the figure. LAI = leaf area index; ET = evapotranspiration; VPD = vapor pressure deficit.

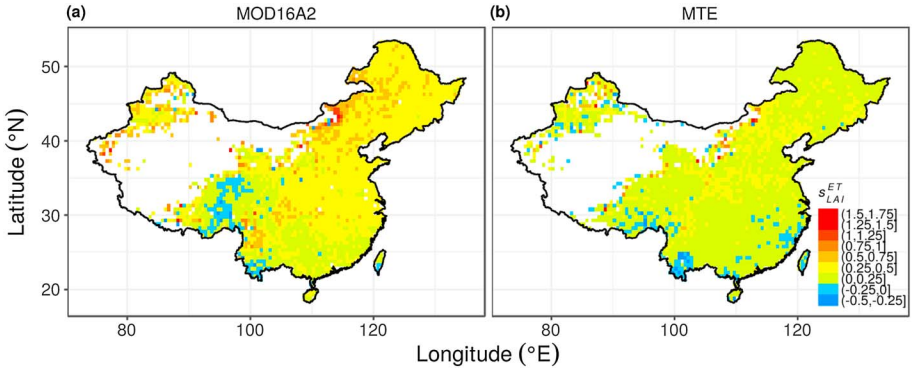

Figure 5. Comparison of the sensitivities of (a) MOD16A2 ET and (b) MTE ET to leaf area index data during 2000–2012. The two products show differences in South China and the Qinghai-Tibet Plateau, where evergreen broadleaf forests and grasslands dominate, respectively. ET = evapotranspiration; MTE = model tree ensemble.

sensitivities were much simpler than those for GPP. The main differences can be seen in the spatial distribution of the variables to which GPP or ET showed the largest sensitivity (Figures 3a and 4a). Among the five predictor variables, ET was most sensitive to radiation or temperature across the majority of China (Figure 4a), whereas GPP was most sensitive to LAI or VPD in parts of the Inner Mongolia Plateau, the Qinghai-Tibet Plateau, and croplands in southwest China (Figure 3a). Opposite to the negative effects of radiation on GPP (Figure 3c) in parts of China, increased radiation generally had a positive effect on ET (Figure 4c). Precipitation also showed positive effects on ET across the majority of China (Figure 4d). Similar to GPP, ET also responded negatively but more moderately to VPD across northern China (Figure 4e). The sensitivities of ET to LAI were positive across most of China, with the exception of parts of tropical and subtropical EBF forests in southern and southwestern China (Figure 4f).. This result contrasts with the previous analysis in the CN-XSH site, where ET responded positively to LAI (Figure 2c). To clarify such dissonance, we compared s^{ET}_{LAI} calculated using MTE ET product during 2000–2010 and that using the MOD16A2 ET product (Mu et al., 2011) in the same period. Figure 5 shows that MOD16A2 produced positive LAI effects on ET in most southern EBF forests and larger s^{ET}_{LAI} in grasslands than the MTE ET product but more negative effects of LAI in the Qinghai-Tibet Plateau. The differences between the results obtained by the two products featured the accuracy or biases of ET products in specific biomes or regions that can affect the spatial sensitivity analysis such as the one conducted in this study.

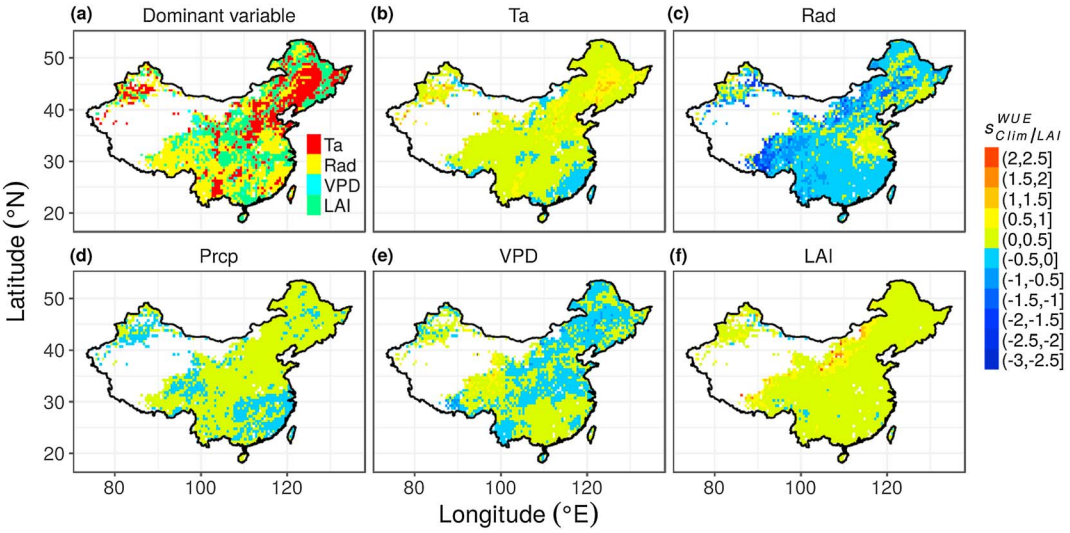

Figure 6. Spatial distribution of (a) variables (climate or LAI) to which WUE is most sensitive and the sensitivities of WUE to monthly variability in (b) air temperature (T_a), (c) solar radiation (Rad), (d) precipitation (Prcp), (e) VPD, and (f) leaf area index (LAI) during 1982–2010. Panel a uses its own categorical legend, while all the other panels share the continuous legend in the right of the figure. LAI = leaf area index; WUE = water use efficiency; VPD = vapor pressure deficit.

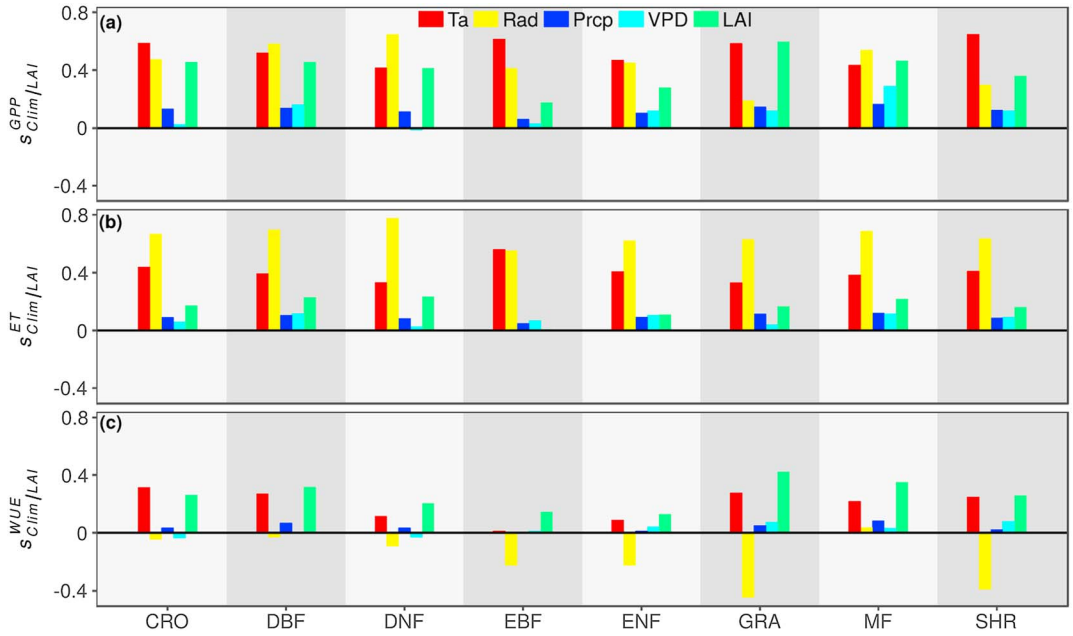

Figure 7. The area-weighted mean sensitivities of (a) GPP, (b) ET, and (c) WUE to monthly variability in climate and LAI during 1982–2010 among different biomes in China. GPP = gross primary productivity; ET = evapotranspiration; WUE = water use efficiency; LAI = leaf area index; VPD = vapor pressure deficit CRO = crops; DBF = deciduous broadleaf forest; DNF = deciduous needle-leaved forest; EBF = evergreen broadleaf forest; ENF = evergreen needle-leaved forest; GRA = grasslands; MF = mixed forests; SHR = shrublands.

WUE was the most sensitive to radiation, LAI, or air temperature in the majority of grid cells (Figure 6a). In grasslands of the Inner Mongolia Plateau and the Qinghai-Tibet Plateau, monthly variability of WUE showed the largest sensitivity to LAI or radiation (Figure 6a). Air temperature generally had positive effects on WUE, in particular in croplands in the northeastern China and parts of grasslands in Xinjiang (Figure 6b). Increasing radiation generally decreased WUE and showed the largest negative effects in grasslands except in parts of the alpine meadows in Xinjiang region (Figure 6c). WUE showed weak negative response to precipitation in parts of Xinjiang due to negative effects of precipitation on GPP and in southeast China due to stronger effects of precipitation on ET (Figures 3d, 4d, and 6d). VPD tended to show weak negative effects on WUE in northern and northeastern China but positive effects in southern China, most of the Qinghai-Tibet Plateau, and parts of Xinjiang (Figure 6e). Similar to GPP, LAI in grasslands in the Inner Mongolia Plateau and Qinghai-Tibet Plateau showed the strongest effects on WUE (Figure 6f).

3.3. Different Responses of Biomes to Climatic Variables and LAI

The area-weighted sensitivities of GPP, ET, and WUE in response to climate and LAI for biomes are summarized in Figure 7. The variable to which GPP was the most sensitive varied among biomes (Figure 7a), while ET across biomes showed the largest sensitivity to radiation except in EBF (Figure 7b). In almost all biomes, WUE showed negative responses to radiation particularly in GRA and SHR (shrublands, Figure 7c). The effects of temperature were generally positive for the change of monthly WUE (Figure 7c) at the biome level. Precipitation and VPD generally showed minor influences across biomes (Figure 7c). While WUE generally responded positively to LAI among biomes, it is noted that WUE of grasslands showed the largest sensitivity to LAI (Figure 7c).

4. Discussion and Conclusions

4.1. Direct Effects of Temperature on GPP, ET, and WUE

Limitations to the rate of photosynthesis include Rubisco enzyme activity, photosynthetic electron transport, and the rate of export or utilization of the photosynthetic products (Collatz et al., 1991; Farquhar et al., 1980). Temperature directly influences the reactions catalyzed by Rubisco and the electron transport chain along with stomatal conductance (discussed in next paragraph); thus, photosynthesis is recognized as a very

temperature-sensitive process (Yamori et al., 2013). The response of photosynthesis to temperature is along a parabolic curve with a peak at an optimum temperature (Berry & Bjorkman, 2003) where plants reach their largest carbon assimilation rate. Therefore, elevated temperature can enhance vegetation productivity when temperature is low but decrease vegetation growth when temperature is too high. For terrestrial ecosystems that have adapted to the current regional climate, the highest monthly temperatures are generally close to the optimal value for maximal rates of photosynthesis (Wan et al., 2005). Thus, GPP generally showed a positive response to increased monthly temperature in either site- or country-level analysis (Figures 2a, 3b, and 7a) because temperatures are frequently lower than the optimal. The positive sensitivity of GPP to temperature was also found in a number of field-warming experiments globally. In a meta-analysis covering various ecosystem types, Lu et al. (2013) reported an on-average 15.7% increase of GPP per 1.81 °C increase in air temperature. However, this positive GPP response to elevated temperature is not temporally homogeneous. Experimental warming in a tall grass prairie in the U.S. Great Plains significantly increased green biomass in spring and autumn but less so in summer (Wan et al., 2005). This contrasting effect of elevated temperature in summer and other seasons has also been found in other ecosystems, including subalpine coniferous forest (Huxman et al., 2003) and white spruce forest in Alaska (Wilmking et al., 2004). It is noted that the direction and magnitude of the sensitivity of GPP to temperature can depend on the magnitude of elevated temperature (Piao et al., 2013). In addition, its impact can be masked by the interactions among temperature and other factors, such as water availability (Niu et al., 2008) and CO_2 concentration (Norby & Luo, 2004). For example, in a temperate grassland near the CN-Xi2 site, experimental warming decreased GPP compared to the control subplots (Niu et al., 2011). However, the increased temperature was accompanied with a significant depletion of soil water, and therefore it is most probable that increased temperature without increased depletion of soil water can increase GPP at this site. As Norby and Luo (2004) noted, the limited number of treatments in factorial experiments often leads to imprecise hypotheses and inconclusive results. This is also the reason that MLR could not distinguish the independent effect of temperature on GPP at the CN-Xi2 site (Figure 2a).

Sources of ET include transpiration by vegetation canopy, soil evaporation, and evaporation from intercepted water by vegetation following rain. Transpiration is regulated by stomatal conductance, which is limited by atmospheric demand for water (usually represented using VPD in practice) and leaf temperature (Bunce, 2000a; Jarvis, 1976; Mott & Peak, 2010). Because leaf temperature and VPD are strongly correlated, it is difficult to conduct factorial experiments outside models (e.g., Eamus, Cleverly, et al., 2013) to distinguish the direct effects of a single variable. However, in the limited number of manipulative experiments reported, stomatal conductance showed a large increase in response to increasing temperature (Fredeen & Sage, 1999; Mott & Peak, 2010). The possible underlying mechanism is that high temperature can decrease water viscosity and increase plant membrane permeability and thus increases water supply to guard cells (Fredeen & Sage, 1999), which will result in higher stomatal conductance and transpiration. In natural environments, maximum stomatal conductance values were found to occur when high temperatures coincided with low VPD in winter wheat and barley crops (Bunce, 2000a). Similarly, Bunce (2000b) reported that stomatal conductance increased exponentially as leaf temperature increased from 15 to 35 °C in eight cool and warm climate herbaceous crop and weed species, even when temperature exceeded the optimum for photosynthesis. Such behavior of stomatal conductance in response to high temperature can benefit plants by cooling leaves in hot environments (Fischer et al., 1998; Lu et al., 1994). However, the temperature increase can drive the increase of VPD, which will lead to the decrease of stomatal conductance and transpiration (Damour et al., 2010). Such a positive direct effect of temperature and the indirect effect of temperature through VPD lead the inflection point of transpiration-VPD curve to be postponed as temperature increases (see Figures 3d and 4a in Fredeen and Sage (1999)). It is noted that the direct effect of temperature on stomatal conductance also influences GPP because vegetation absorbs CO_2 from the atmosphere through stomata.

We found that WUE showed varied temperature sensitivities among biomes due to the differences between the responses of GPP and ET to temperature. This arises from biomes that have (a) different optimum temperatures for GPP (Berry & Bjorkman, 2003; Yamori et al., 2013), (b) different acclimation capacities to temperature (Smith et al., 2016; Yamori et al., 2013), and (c) different increased stomatal conductance with elevated temperature (Bunce, 2000a, 2000b; Fredeen & Sage, 1999; Mott & Peak, 2010).

4.2. Direct Effects of Radiation on GPP, ET, and WUE

Radiation directly regulates rates of photosynthetic electron transport (Farquhar & Sharkey, 2003; Tinocoojanguren & Pearcy, 1993) and stomatal behavior (Hattori et al., 2007; Tinocoojanguren & Pearcy, 1993). Stomatal conductance can respond rapidly to sudden change in light intensity (Hattori et al., 2007; Tinocoojanguren & Pearcy, 1993). Generally, the response of rates of photosynthesis to radiation can be described by a rectangular hyperbolic curve (Yu et al., 2004). However, excessive radiation can induce injury to the photosynthetic apparatus (hereafter photoinhibition, Powles, 2003; Warner & Caldwell, 1983), including photodestruction of photosynthetic pigments and even cell death. This is likely to be the reason that GPP showed a negative response to radiation in parts of Inner Mongolia Plateau and Qinghai-Tibet Plateau (Figure 3c) and relatively low radiation sensitivity in grasslands compared to other biomes (Figure 7a). However, the occurrence of photoinhibition is not related to the degree of stomatal opening (Powles, 2003). Jones (1998) reported that carbon assimilation of *Phaseolus* leaves was stable while stomatal conductance continued to rise as light intensity increased. Therefore, strong radiation showed minor negative effects on ET (Figure 4c). Furthermore, increased radiation can stimulate evaporation from the soil surface and from wet canopies. This is likely to be the reason that ET generally showed larger radiation sensitivities than GPP among biomes, and thus WUE showed negative response to elevated radiation (Figure 7c).

4.3. Direct Effects of Water Availability on GPP, ET, and WUE

Increased frequency, severity, and areal extent of droughts have been widely reported across the world (Allen et al., 2010; Carnicer et al., 2011; Matusick et al., 2013). In extreme cases, severe water stress can lead to large-scale mortality of trees (Hicke et al., 2012; Phillips et al., 2009). Water stress decreases stomatal conductance (Jarvis, 1976; Lu & Zhang, 1999; Zhou et al., 2014) and can affect photosynthetic biochemical processes (Graan & Boyer, 1990; Zhou et al., 2013). Accompanied with depression of GPP, canopy transpiration declines due to stomatal closure. These effects of water stress can reasonably explain the positive responses of GPP and ET to increasing precipitation at the site level (Figure 2), in the majority of China (Figures 3 and 4) and among biomes (Figure 7). However, the effects of water availability can be masked by other covarying factors. For example, at the alpine meadow (CN-Ha2) which is generally thought of as temperature-limited (Guo et al., 2015), the PLSR-based algorithm obtained a positive sensitivity of GPP to precipitation (Figure 2a), whereas the MLR model estimated no significant response to precipitation (Figure 2b). However, at this site Guo et al. (2015) showed that water availability can mediate the effects of increasing temperature on GPP (Figure 4a in the paper), that is, the positive effect of high SWC on GPP partly offsets the negative effect of low temperature. Therefore, the MLR model failed to reveal the precipitation effect on GPP. Although GPP and ET usually respond positively to increasing water availability, excessive SWC can result in down regulation of stomatal conductance and photosynthesis arising from root zone hypoxia (Bradford, 1983; Merchant et al., 2010; Pociecha et al., 2008). For example, the negative effects of growing season precipitation or large rainfall events on vegetation growth in alpine meadows or grasslands in parts of Xinjiang, Inner Mongolia Plateau, and Qinghai-Tibet Plateau (Figure 3d) were also reported by Piao et al. (2006) and Yuan et al. (2015). They attributed the negative effects of precipitation on vegetation growth to simultaneous decrease in temperature (Piao et al., 2006; Yuan et al., 2015), although extensive precipitation is also associated with reduced solar radiation inputs which may also contribute to reduced GPP. It has been reported that unusually large rainfall events can reduce aboveground productivity by vegetation in comparison to average rainfall events (Knapp et al., 2002; Xu & Zhou, 2011). As for Xinjiang and other semiarid regions in China, grassland ecosystems are widely distributed in mountain areas where water limitation is not as severe as commonly expected in other arid and semiarid regions. The photosynthesis of local dominant species *Leymus chinensis* and *Stipa grandis* are found to be enhanced under moderate SWC but reduced under severe water deficit and excessive water (Xu & Zhou, 2011). In light of such negative effects of precipitation on vegetation growth, more efforts are needed to address whether and to what degree grassland ecosystems in above regions can benefit from the climate change-induced shifts of precipitation amount and pattern.

4.4. Direct Effects of VPD on GPP, ET, and WUE

The influence of VPD on leaf stomatal conductance and thus GPP, ET, and WUE has been extensively studied (e.g., Lange et al., 1971; Leuning, 1995; Monteith, 1995; Shi et al., 2014; Thomas & Eamus, 1999). It is widely recognized that leaf stomatal conductance could increase as VPD increases when VPD is low or moderate but decrease with increasing VPD when it is high (Damour et al., 2010). At the ecosystem level, a number

of studies have reported the close correlations between GPP, ET, or WUE and VPD (Eamus, Boulain, et al., 2013; Ponton et al., 2006; Shi et al., 2014; F. M. Zhang et al., 2013). Our results (Figures 2, 3d, 4d, 6d, and 7) are consistent with these previous studies. However, it is noted that the sensitivity of vegetation to VPD can be mediated by other factors such as soil water stress (Cunningham, 2005; Niglas et al., 2014; Thomas & Eamus, 1999). In addition, in a condition of high humidity, the reduced evaporative demand of the atmosphere could contribute to the less sensitivity of ET to elevated VPD than that of GPP and thus causes a positive response of WUE in ecosystems in northern and northeastern China (Figures 2e and 7c) (Frank et al., 2015).

4.5. Direct Effects of LAI on GPP, ET, and WUE

Although there were uncertainties induced by the accuracy of data sets used in this study (e.g., Figure 5 as discussed later), the results showed that LAI generally exerted positive effects on GPP, ET, and WUE (Figures 3f, 4f, 6f, and 7). Structural dynamics can influence the biophysical properties of vegetation and carbon, water, and energy fluxes (Bonan, 1993). Changes in the magnitude and distribution of LAI can affect the absorbance of photosynthetically active radiation (Nilson, 1971) and the partitioning of net radiation between sensible and latent heat flux (Verstraete & Dickinson, 1986). Numerous studies have documented the strong positive control of GPP exerted by LAI, especially in biomes with a low-to-moderate LAI (Duursma et al., 2009; Keith et al., 2012; Van Dijk et al., 2005). Large values of LAI can result in a decrease of GPP (e.g., EBF forests in southwest China and in southern Tibet) due to a higher proportion of aged leaves with low assimilation capacity (Joggi et al., 1983) and through self-shading of leaves within the canopy. The positive effects of LAI on ET are more significant in influencing seasonality of ET but weak on long-term ET, because it is energy and water availability that control annual ET (Kabat et al., 1997; Liu et al., 1992). Analysis by a process-based model showed that LAI has stronger effects on GPP than ET (Puma et al., 2013); thus, the sensitivity of WUE to LAI is positive among biomes and is particularly large in grasslands (Figure 7c). This result is consistent with the report by Hu et al. (2008) that the seasonality of WUE at four grassland sites in the Qinghai-Tibet Plateau and North China were controlled by LAI.

4.6. Uncertainties and Implications

The data sets used in the spatial analysis were developed from interpolation of meteorological measurements (climate variables), satellite monitoring (LAI), and data-driven products upscaled from the FLUXNET observations (GPP and ET). Therefore, there exist unavoidable uncertainties. The comparison of responses of MTE ET and MOD16A2 ET to LAI (Figure 5) shows that these uncertainties can bring subtle influences to the results. The lack of long-term continuous eddy covariance observations, particularly in tropical and subtropical EBF forests (most FLUXNET sites are from temperate regions), means that the MTE products have to use spatial relationships to derive temporal variations (Piao et al., 2013). However, the spatial relationships are not totally equal to the temporal relationships and thus could bring considerable uncertainty.

Although uncertainties exist, the PLSR-based algorithm performed better than the conventional MLR model for monthly GPP, ET, and WUE, providing reasonable estimates of the individual effects of climate variables and LAI which highly covary with each other. Our results can inform the design of field experiments that try to discern the influences of multiple factors. It is often technologically impractical and expensive in both financial and time costs to conduct factorial experiments at the ecosystem level. The PLSR-based algorithm allows discrimination of the most important variables driving GPP, ET, and WUE. It can also be used to assess the accuracy of data-driven products and clarify which factor is not appropriately represented in the product, as identified in our comparison of MTE ET and MOD16A2 ET products. Third, our results can be used to evaluate the performance of complex ecosystem models in response to a single variable through factorial simulations, which are usually validated by field experiments at the ecosystem scale.

Acknowledgments
We thank researchers from the ChinaFlux community for data sharing. Y. Li and S. Wang are supported by the Ministry of Science and Technology of China (2016YFA0600202). H. Shi and Q. Yu are supported by Northwest A & F University of China (A314021403-C4). S. Wang is supported by the National Natural Science Foundation of China (41571192). L. Zhou is supported by the National Natural Science Foundation of China (41401110). There are no conflicts of interest related to this work. The eddy covariance data and meteorological data are acquired from CNERN (http://www.cnern.org.cn/). The monthly MTE GPP and ET products were downloaded from the Department of Biogeochemical Integration (BGI) of MPI (http://www.bgc-jena.mpg.de/geo-db/projects/Data.php). The monthly climate data can be obtained from the webpage (https://vesg.ipsl.upmc.fr/thredds/catalog/work/p529viov/cruncep/V8_1901_2016/catalog.html). The GLOBMAP v3.0 LAI data were downloaded from http://modis.cn/globalLAI/.

References

Ainsworth, E. A., & Rogers, A. (2007). The response of photosynthesis and stomatal conductance to rising CO_2: Mechanisms and environmental interactions. *Plant, Cell & Environment*, *30*(3), 258–270. https://doi.org/10.1111/j.1365-3040.2007.01641.x

Allen, C. D., Macalady, A. K., Chenchouni, H., Bachelet, D., Mcdowell, N., Vennetier, M., et al. (2010). A global overview of drought and heat-induced tree mortality reveals emerging climate change risks for forests. *Forest Ecology and Management*, *259*(4), 660–684. https://doi.org/10.1016/j.foreco.2009.09.001

Bai, Y., Wu, J., Xing, Q., Pan, Q., Huang, J., Yang, D., & Han, X. (2008). Primary production and rain use efficiency across a precipitation gradient on the Mongolia Plateau. *Ecology*, *89*(8), 2140–2153. https://doi.org/10.1890/07-0992.1

Berry, J., & Bjorkman, O. (2003). Photosynthetic response and adaptation to temperature in higher plants. *Annual Review of Plant Biology*, *31*(1), 491–543.

Bonan, G. B. (1993). Importance of leaf area index and forest type when estimating photosynthesis in boreal forests. *Remote Sensing of Environment*, *43*(3), 303–314. https://doi.org/10.1016/0034-4257(93)90072-6

Bradford, K. J. (1983). Effects of soil flooding on leaf gas exchange of tomato plants. *Plant Physiology*, *73*(2), 475–479. https://doi.org/10.1104/pp.73.2.475

Brümmer, C., Black, T. A., Jassal, R. S., Grant, N. J., Spittlehouse, D. L., Chen, B., et al. (2012). How climate and vegetation type influence evapotranspiration and water use efficiency in Canadian forest, peatland and grassland ecosystems. *Agricultural and Forest Meteorology*, *153*, 14–30. https://doi.org/10.1016/j.agrformet.2011.04.008

Bunce, J. A. (2000a). Responses of stomatal conductance to light, humidity and temperature in winter wheat and barley grown at three concentrations of carbon dioxide in the field. *Global Change Biology*, *6*(4), 371–382. https://doi.org/10.1046/j.1365-2486.2000.00314.x

Bunce, J. A. (2000b). Acclimation of photosynthesis to temperature in eight cool and warm climate herbaceous C_3 species: Temperature dependence of parameters of a biochemical photosynthesis model. *Photosynthesis Research*, *63*(1), 59–67. https://doi.org/10.1023/A:1006325724086

Campos, G. E. P., Moran, M. S., Huete, A., Zhang, Y. G., Bresloff, C., Huxman, T. E., et al. (2013). Ecosystem resilience despite large-scale altered hydroclimatic conditions. *Nature*, *494*(7437), 349–352. https://doi.org/10.1038/nature11836

Carnicer, J., Coll, M., Ninyerola, M., Pons, X., Sanchez, G., & Penuelas, J. (2011). Widespread crown condition decline, food web disruption, and amplified tree mortality with increased climate change-type drought. *Proceedings of the National Academy of Sciences of the United States of America*, *108*(4), 1474–1478. https://doi.org/10.1073/pnas.1010070108

Collatz, G. J., Ball, J. T., Grivet, C., & Berry, J. A. (1991). Physiological and environmental regulation of stomatal conductance, photosynthesis and transpiration: A model that includes a laminar boundary layer. *Agricultural and Forest Meteorology*, *54*(2–4), 107–136. https://doi.org/10.1016/0168-1923(91)90002-8

Cunningham, S. C. (2005). Photosynthetic responses to vapour pressure deficit in temperate and tropical evergreen rainforest trees of Australia. *Oecologia*, *142*(4), 521–528. https://doi.org/10.1007/s00442-004-1766-1

Damour, G., Simonneau, T., Cochard, H., & Urban, L. (2010). An overview of models of stomatal conductance at the leaf level. *Plant, Cell & Environment*, *33*(9), 1419–1438.

Duursma, R. A., Kolari, P., Peramaki, M., Pulkkinen, M., Makela, A., Nikinmaa, E., et al. (2009). Contributions of climate, leaf area index and leaf physiology to variation in gross primary production of six coniferous forests across Europe: A model-based analysis. *Tree Physiology*, *29*(5), 621–639. https://doi.org/10.1093/treephys/tpp010

Eamus, D., Boulain, N., Cleverly, J., & Breshears, D. D. (2013). Global change-type drought-induced tree mortality: Vapor pressure deficit is more important than temperature per se in causing decline in tree health. *Ecology and Evolution*, *3*(8), 2711–2729. https://doi.org/10.1002/ece3.664

Eamus, D., Cleverly, J., Boulain, N., Grant, N., Faux, R., & Villalobos-Vega, R. (2013). Carbon and water fluxes in an arid-zone Acacia savanna woodland: An analyses of seasonal patterns and responses to rainfall events. *Agricultural and Forest Meteorology*, *182-183*(22), 225–238.

Farquhar, G. D., & Sharkey, T. D. (2003). Stomatal conductance and photosynthesis. *Annual Review of Plant Biology*, *33*(1), 317–345.

Farquhar, G. D., Von Caemmerer, S., & Berry, J. A. (1980). A biochemical model of photosynthetic CO_2 assimilation in leaves of C_3 species. *Planta*, *149*(1), 78–90. https://doi.org/10.1007/BF00386231

Fischer, R. A., Rees, D., Sayre, K. D., Lu, Z. M., Condon, A. G., & Saavedra, A. L. (1998). Wheat yield progress associated with higher stomatal conductance and photosynthetic rate, and cooler canopies. *Crop Science*, *38*(6), 1467–1475. https://doi.org/10.2135/cropsci1998.0011183X003800060011x

Frank, D. C., Poulter, B., Saurer, M., Esper, J., Huntingford, C., Helle, G., et al. (2015). Water-use efficiency and transpiration across European forests during the Anthropocene. *Nature Climate Change*, *5*(6), 579–583. https://doi.org/10.1038/nclimate2614

Fredeen, A. L., & Sage, R. F. (1999). Temperature and humidity effects on branchlet gas-exchange in white spruce: An explanation for the increase in transpiration with branchlet temperature. *Trees-Structure and Function*, *14*(3), 0161. https://doi.org/10.1007/s004680050220

Graan, T., & Boyer, J. S. (1990). Very high CO_2 partially restores photosynthesis in sunflower at low water potentials. *Planta*, *181*(3), 378–384. https://doi.org/10.1007/BF00195891

Graham, M. H. (2003). Confronting multicollinearity in ecological multiple regression. *Ecology*, *84*(11), 2809–2815. https://doi.org/10.1890/02-3114

Guo, Q., Hu, Z. M., Li, S. G., Yu, G. R., Sun, X. M., Zhang, L. M., et al. (2015). Contrasting responses of gross primary productivity to precipitation events in a water-limited and a temperature-limited grassland ecosystem. *Agricultural and Forest Meteorology*, *214*, 169–177.

Hattori, T., Sonobe, K., Inanaga, S., An, P., Tsuji, W., Araki, H., et al. (2007). Short term stomatal responses to light intensity changes and osmotic stress in sorghum seedlings raised with and without silicon. *Environmental and Experimental Botany*, *60*(2), 177–182. https://doi.org/10.1016/j.envexpbot.2006.10.004

Hicke, J. A., Allen, C. D., Desai, A. R., Dietze, M. C., Hall, R. J., Hogg, E. H., et al. (2012). Effects of biotic disturbances on forest carbon cycling in the United States and Canada. *Global Change Biology*, *18*(1), 7–34. https://doi.org/10.1111/j.1365-2486.2011.02543.x

Hu, Z. M., Yu, G. R., Fu, Y. L., Sun, X. M., Li, Y. N., Shi, P. L., et al. (2008). Effects of vegetation control on ecosystem water use efficiency within and among four grassland ecosystems in China. *Global Change Biology*, *14*(7), 1609–1619. https://doi.org/10.1111/j.1365-2486.2008.01582.x

Huang, M. T., Piao, S. L., Sun, Y., Ciais, P., Cheng, L., Mao, J. F., et al. (2015). Change in terrestrial ecosystem water-use efficiency over the last three decades. *Global Change Biology*, *21*(6), 2366–2378. https://doi.org/10.1111/gcb.12873

Huang, M. T., Piao, S. L., Zeng, Z. Z., Peng, S. S., Ciais, P., Cheng, L., et al. (2016). Seasonal responses of terrestrial ecosystem water-use efficiency to climate change. *Global Change Biology*, *22*(6), 2165–2177. https://doi.org/10.1111/gcb.13180

Huxman, T. E., Turnipseed, A. A., Sparks, J. P., Harley, P., & Monson, R. K. (2003). Temperature as a control over ecosystem CO_2 fluxes in a high-elevation, subalpine forest. *Oecologia*, *134*(4), 537–546. https://doi.org/10.1007/s00442-002-1131-1

Jarvis, P. G. (1976). The interpretation of the variations in leaf water potential and stomatal conductance found in canopies in the field. *Philosophical Transactions of the Royal Society of London, Series B*, *273*(927), 593–610. https://doi.org/10.1098/rstb.1976.0035

Joggi, D., Hofer, U., & Nosberger, J. (1983). Leaf area index, canopy structure and photosynthesis of red clover (*Trifolium pratense* L.). *Plant, Cell & Environment*, *6*(8), 611–616.

Jones, H. G. (1998). Stomatal control of photosynthesis and transpiration. *Journal of Experimental Botany*, *49*(Special), 387–398. https://doi.org/10.1093/jxb/49.Special_Issue.387

Jung, M., Reichstein, M., & Bondeau, A. (2009). Towards global empirical upscaling of FLUXNET eddy covariance observations: Validation of a model tree ensemble approach using a biosphere model. *Biogeosciences*, *6*(10), 2001–2013.

Jung, M., Reichstein, M., Margolis, H. A., Cescatti, A., Richardson, A. D., Arain, M. A., et al. (2011). Global patterns of land-atmosphere fluxes of carbon dioxide, latent heat, and sensible heat derived from eddy covariance, satellite, and meteorological observations. *Journal of Geophysical Research*, *116*, G00J07. https://doi.org/10.1029/2010JG001566

Kabat, P., Dolman, A. J., & Elbers, J. A. (1997). Evaporation, sensible heat and canopy conductance of fallow savannah and patterned woodland in the Sahel. *Journal of Hydrology*, *188*, 494–515.

Keenan, T. F., Hollinger, D. Y., Bohrer, G., Dragoni, D., Munger, J. W., Schmid, H. P., & Richardson, A. D. (2013). Increase in forest water-use efficiency as atmospheric carbon dioxide concentrations rise. *Nature*, *499*(7458), 324–327. https://doi.org/10.1038/nature12291

Keith, H., Van Gorsel, E., Jacobsen, K. L., & Cleugh, H. A. (2012). Dynamics of carbon exchange in a Eucalyptus forest in response to interacting disturbance factors. *Agricultural and Forest Meteorology*, *153*, 67–81. https://doi.org/10.1016/j.agrformet.2011.07.019

Knapp, A. K., Fay, P. A., Blair, J. M., Collins, S. L., Smith, M. D., Carlisle, J. D., et al. (2002). Rainfall variability, carbon cycling and plant species diversity in a mesic grassland. *Science*, *298*(5601), 2202–2205. https://doi.org/10.1126/science.1076347

Lange, O. L., Losch, R., Schulze, E. D., & Kappen, L. (1971). Responses of stomata to changes in humidity. *Planta*, *100*(1), 76–86. https://doi.org/10.1007/BF00386887

Law, B. E., Falge, E., Gu, L., Baldocchi, D. D., Bakwin, P., Berbigier, P., et al. (2002). Environmental controls over carbon dioxide and water vapor exchange of terrestrial vegetation. *Agricultural and Forest Meteorology*, *113*(1–4), 97–120. https://doi.org/10.1016/S0168-1923(02)00104-1

Leuning, R. (1995). A critical appraisal of a combined stomatal-photosynthesis model for C_3 plants. *Plant, Cell & Environment*, *18*(4), 339–355. https://doi.org/10.1111/j.1365-3040.1995.tb00370.x

Li, S. G., Eugster, W., Asanuma, J., Kotani, A., Davaa, G., Oyunbaatar, D., et al. (2008). Response of gross ecosystem productivity, light use efficiency, and water use efficiency of Mongolian steppe to seasonal variations in soil moisture. *Journal of Geophysical Research*, *113*, G01019. https://doi.org/10.1029/2006jg000349

Lindroth, A., & Cienciala, E. (1996). Water use efficiency of short-rotation *Salix viminalis* at leaf, tree and stand scales. *Tree Physiology*, *16*(1–2), 257–262. https://doi.org/10.1093/treephys/16.1-2.257

Liu, Y., Liu, R., & Chen, J. M. (2012). Retrospective retrieval of long-term consistent global leaf area index (1981–2011) from combined AVHRR and MODIS data. *Journal of Geophysical Research*, *117*, G04003. https://doi.org/10.1029/2012JG002084

Liu, Y. Q., Ye, D. Z., & Ji, J. J. (1992). Influence of soil moisture and vegetation on climate (I): Theoretical analysis to persistence of short-term climate anomalies. *SCIENCE CHINA Chemistry*, *35*(12), 1485–1493.

Lu, C. M., & Zhang, J. H. (1999). Effects of water stress on photosystem II photochemistry and its thermostability in wheat plants. *Journal of Experimental Botany*, *50*(336), 1199–1206. https://doi.org/10.1093/jxb/50.336.1199

Lu, M., Zhou, X. H., Yang, Q., Li, H., Luo, Y. Q., Fang, C. M., et al. (2013). Responses of ecosystem carbon cycle to experimental warming: A meta-analysis. *Ecology*, *94*(3), 726–738. https://doi.org/10.1890/12-0279.1

Lu, Z., Radin, J. W., Turcotte, E. L., Percy, R. G., & Zeiger, E. (1994). High yields in advanced lines of Pima cotton are associated with higher stomatal conductance, reduced leaf area and lower leaf temperature. *Plant Physiology*, *92*(2), 266–272. https://doi.org/10.1111/j.1399-3054.1994.tb05336.x

Mastrotheodoros, T., Pappas, C., Molnar, P., Burlando, P., Keenan, T. F., Gentine, P., et al. (2017). Linking plant functional trait plasticity and the large increase in forest water use efficiency. *Journal of Geophysical Research: Biogeosciences*, *122*, 2393–2408. https://doi.org/10.1002/2017JG003890

Matusick, G., Ruthrof, K., Brouwers, N. C., Dell, B., & Hardy, G. (2013). Sudden forest canopy collapse corresponding with extreme drought and heat in a Mediterranean-type eucalypt forest in southwestern Australia. *European Journal of Forest Research*, *132*(3), 497–510. https://doi.org/10.1007/s10342-013-0690-5

Merchant, A., Peuke, A. D., Keitel, C., Macfarlane, C., Warren, C. R., & Adams, M. A. (2010). Phloem sap and leaf $\delta^{13}C$, carbohydrates and amino acid concentrations in *Eucalyptus globulus* change systematically according to flooding and water deficit treatment. *Journal of Experimental Botany*, *61*(6), 1785–1793. https://doi.org/10.1093/jxb/erq045

Mevik, B. H., & Wehrens, R. (2007). The pls package: Principal component and partial least squares regression in R. *Journal of Statistical Software*, *18*(2), 1–23.

Monteith, J. L. (1995). A reinterpretation of stomatal responses to humidity. *Plant, Cell & Environment*, *18*(4), 357–364. https://doi.org/10.1111/j.1365-3040.1995.tb00371.x

Mott, K. A., & Peak, D. (2010). Stomatal responses to humidity and temperature in darkness. *Plant, Cell & Environment*, *33*(7), 1084–1090.

Mu, Q., Zhao, M., & Running, S. W. (2011). Improvements to a MODIS global terrestrial evapotranspiration algorithm. *Remote Sensing of Environment*, *115*(8), 1781–1800. https://doi.org/10.1016/j.rse.2011.02.019

Niglas, A., Kupper, P., Tullus, A., & Sellin, A. (2014). Responses of sap flow, leaf gas exchange and growth of hybrid aspen to elevated atmospheric humidity under field conditions. *Aob Plants*, *6*. https://doi.org/10.1093/aobpla/plu021

Nilson, T. (1971). A theoretical analysis of the frequency of gaps in plant stands. *Agricultural Meteorology*, *8*(71), 25–38. https://doi.org/10.1016/0002-1571(71)90092-6

Niu, S. L., Wu, M. Y., Han, Y., Xia, J. Y., Li, L. H., & Wan, S. Q. (2008). Water-mediated responses of ecosystem carbon fluxes to climatic change in a temperate steppe. *New Phytologist*, *177*(1), 209–219. https://doi.org/10.1111/j.1469-8137.2007.02237.x

Niu, S. L., Xing, X. R., Zhang, Z., Xia, J. Y., Zhou, X. H., Song, B., et al. (2011). Water-use efficiency in response to climate change: From leaf to ecosystem in a temperate steppe. *Global Change Biology*, *17*(2), 1073–1082. https://doi.org/10.1111/j.1365-2486.2010.02280.x

Norby, R. J., & Luo, Y. (2004). Evaluating ecosystem responses to rising atmospheric CO_2 and global warming in a multi-factor world. *New Phytologist*, *162*(2), 281–293. https://doi.org/10.1111/j.1469-8137.2004.01047.x

Norby, R. J., & Zak, D. R. (2011). Ecological lessons from Free-Air CO_2 Enrichment (FACE) experiments. *Annual Review of Ecology Evolution and Systematics*, *42*(1), 181–203. https://doi.org/10.1146/annurev-ecolsys-102209-144647

Phillips, O. L., Aragao, L. E. O. C., Lewis, S. L., Fisher, J. B., Lloyd, J., Lopez-Gonzalez, G., et al. (2009). Drought sensitivity of the Amazon rainforest. *Science*, *323*(5919), 1344–1347. https://doi.org/10.1126/science.1164033

Piao, S. L., Mohammat, A., Fang, J. Y., Cai, Q., & Feng, J. M. (2006). NDVI-based increase in growth of temperate grasslands and its responses to climate changes in China. *Global Environmental Change*, *16*(4), 340–348. https://doi.org/10.1016/j.gloenvcha.2006.02.002

Piao, S. L., Sitch, S., Ciais, P., Friedlingstein, P., Peylin, P., Wang, X. H., et al. (2013). Evaluation of terrestrial carbon cycle models for their response to climate variability and to CO_2 trends. *Global Change Biology*, *19*(7), 2117–2132. https://doi.org/10.1111/gcb.12187

Pociecha, E., Kościelniak, J., & Filek, W. (2008). Effects of root flooding and stage of development on the growth and photosynthesis of field bean (*Vicia faba* L. minor). *Acta Physiologiae Plantarum*, *30*(4), 529–535. https://doi.org/10.1007/s11738-008-0151-9

Ponton, S., Flanagan, L. B., Alstad, K. P., Johnson, B. G., Morgenstern, K., Kljun, N., et al. (2006). Comparison of ecosystem water-use efficiency among Douglas-fir forest, aspen forest and grassland using eddy covariance and carbon isotope techniques. *Global Change Biology*, *12*(2), 294–310. https://doi.org/10.1111/j.1365-2486.2005.01103.x

Powles, S. B. (2003). Photoinhibition of photosynthesis induced by visible light. *Annual Review of Plant Biology*, *35*(1), 15–44.
Puma, M. J., Koster, R. D., & Cook, B. I. (2013). Phenological versus meteorological controls on land-atmosphere water and carbon fluxes. *Journal of Geophysical Research-Biogeosciences*, *118*, 14–29. https://doi.org/10.1029/2012JG002088
Quan, Q., Zhang, F. Y., Tian, D. S., Zhou, Q. P., Wang, L. X., & Niu, S. L. (2018). Transpiration dominates ecosystem water-use efficiency in response to warming in an alpine meadow. *Journal of Geophysical Research: Biogeosciences*, *123*, 453–462. https://doi.org/10.1002/2017JG004362
Raupach, M. R., Haverd, V., & Briggs, P. R. (2013). Sensitivities of the Australian terrestrial water and carbon balances to climate change and variability. *Agricultural and Forest Meteorology*, *182-183*, 277–291. https://doi.org/10.1016/j.agrformet.2013.06.017
Reichstein, M., Tenhunen, J. D., Roupsard, O., Ourcival, J. M., Rambal, S., Miglietta, F., et al. (2002). Severe drought effects on ecosystem CO_2 and H_2O fluxes at three Mediterranean evergreen sites: Revision of current hypotheses? *Global Change Biology*, *8*(10), 999–1017. https://doi.org/10.1046/j.1365-2486.2002.00530.x
Shi, H., Li, L., Eamus, D., Cleverly, J., Huete, A. R., Beringer, J., et al. (2014). Intrinsic climate dependency of ecosystem light and water-use-efficiencies across Australian biomes. *Environmental Research Letters*, *9*(10), 104,002. https://doi.org/10.1088/1748-9326/9/10/104002
Smith, N. G., Malyshev, S., Shevliakova, E., Kattge, J., & Dukes, J. S. (2016). Foliar temperature acclimation reduces simulated carbon sensitivity to climate. *Nature Climate Change*, *6*(4), 407–411. https://doi.org/10.1038/nclimate2878
Tan, Z. H., Cao, M., Yu, G. R., Tang, J. W., Deng, X. B., Song, Q. H., et al. (2013). High sensitivity of a tropical rainforest to water variability: Evidence from 10 years of inventory and eddy flux data. *Journal of Geophysical Research*, *118*, 9393–9400. https://doi.org/10.1002/jgrd.50675
Thomas, D. S., & Eamus, D. (1999). The influence of predawn leaf water potential on stomatal responses to atmospheric water content at constant Ci and on stem hydraulic conductance and foliar ABA concentrations. *Journal of Experimental Botany*, *50*(331), 243–251. https://doi.org/10.1093/jxb/50.331.243
Tinocoojanguren, C., & Pearcy, R. W. (1993). Stomatal dynamics and its importance to carbon gain in two rainforest *Piper* species: II. Stomatal versus biochemical limitations during photosynthetic induction. *Oecologia*, *94*(3), 395–402. https://doi.org/10.1007/BF00317115
Van Dijk, A. I. J. M., Dolman, A. J., & Schulze, E. (2005). Radiation, temperature, and leaf area explain ecosystem carbon fluxes in boreal and temperate European forests. *Global Biogeochemical Cycles*, *19*, GB2029. https://doi.org/10.1029/2004GB002417
Verstraete, M., & Dickinson, R. E. (1986). Modeling surface processes in atmospheric general circulation models. *Annales Geophysicae*, *4*(4), 357–364.
Wan, S. Q., Hui, D. F., Wallace, L., & Luo, Y. Q. (2005). Direct and indirect effects of experimental warming on ecosystem carbon processes in a tallgrass prairie. *Global Biogeochemical Cycles*, *19*, GB2014. https://doi.org/10.1029/2004GB002315
Warner, C. W., & Caldwell, M. M. (1983). Influence of photon flux density in the 400–700 nm waveband on inhibition of photosynthesis by UV-B (280–320 nm) irradiation in soybean leaves: Separation of indirect and immediate effects. *Photochemistry and Photobiology*, *38*(3), 341–346. https://doi.org/10.1111/j.1751-1097.1983.tb02681.x
Wei, Y., Liu, S. V., Huntzinger, D. N., Michalak, A. M., Viovy, N., Post, W. M., et al. (2014). The North American Carbon Program Multi-scale Synthesis and Terrestrial Model Intercomparison Project—Part 2: Environmental driver data. *Geoscientific Model Development*, *7*(6), 2875–2893. https://doi.org/10.5194/gmd-7-2875-2014
Wilmking, M., Juday, G. P., Barber, V., & Zald, H. S. J. (2004). Recent climate warming forces contrasting growth responses of white spruce at treeline in Alaska through temperature thresholds. *Global Change Biology*, *10*(10), 1724–1736. https://doi.org/10.1111/j.1365-2486.2004.00826.x
Wu, B. F., Yuan, Q. Z., Yan, C. Z., Wang, Z. M., Yu, X. F., Li, A. N., et al. (2014). Land cover changes of China from 2000 to 2010. *Quaternary Science*, *34*(4), 723–731.
Xu, Z. Z., & Zhou, G. S. (2011). Responses of photosynthetic capacity to soil moisture gradient in perennial rhizome grass and perennial bunchgrass. *BMC Plant Biology*, *11*(1), 21–21. https://doi.org/10.1186/1471-2229-11-21
Yamori, W., Hikosaka, K., & Way, D. A. (2013). Temperature response of photosynthesis in C_3, C_4, and CAM plants: Temperature acclimation and temperature adaptation. *Photosynthesis Research*, *119*, 101–117.
Yu, G. R., Song, X., Wang, Q. F., Liu, Y. F., Guan, D. X., Yan, J. H., et al. (2008). Water-use efficiency of forest ecosystems in eastern China and its relations to climatic variables. *New Phytologist*, *177*(4), 927–937. https://doi.org/10.1111/j.1469-8137.2007.02316.x
Yu, G. R., Wen, X. F., Sun, X. M., Tanner, B. D., Lee, X. H., & Chen, J. Y. (2006). Overview of ChinaFLUX and evaluation of its eddy covariance measurement. *Agricultural and Forest Meteorology*, *137*(3-4), 125–137. https://doi.org/10.1016/j.agrformet.2006.02.011
Yu, Q., Zhang, Y., Liu, Y., & Shi, P. (2004). Simulation of the stomatal conductance of winter wheat in response to light, temperature and CO_2 changes. *Annals of Botany*, *93*(4), 435–441. https://doi.org/10.1093/aob/mch023
Yuan, X. L., Li, L. H., Chen, X., & Shi, H. (2015). Effects of precipitation intensity and temperature on NDVI-based grass change over northern China during the period from 1982 to 2011. *Remote Sensing*, *7*(8), 10,164–10,183. https://doi.org/10.3390/rs70810164
Zhang, F. M., Ju, W. M., Shen, S. H., Wang, S. Q., Yu, G. R., & Han, S. J. (2013). How recent climate change influences water use efficiency in East Asia. *Theoretical and Applied Climatology*, *116*(1), 359–370.
Zhang, J. H., Hu, Y. L., Xiao, X., Chen, P., Han, S. J., Song, G., et al. (2009). Satellite-based estimation of evapotranspiration of an old-growth temperate mixed forest. *Agricultural and Forest Meteorology*, *149*(6-7), 976–984. https://doi.org/10.1016/j.agrformet.2008.12.002
Zhou, S., Duursma, R. A., Medlyn, B. E., Kelly, J. W. G., & Prentice, I. C. (2013). How should we model plant responses to drought? An analysis of stomatal and non-stomatal responses to water stress. *Agricultural and Forest Meteorology*, *182–183*(22), 204–214.
Zhou, S., Medlyn, B., Sabate, S., Sperlich, D., & Prentice, I. C. (2014). Short-term water stress impacts on stomatal, mesophyll and biochemical limitations to photosynthesis differ consistently among tree species from contrasting climates. *Tree Physiology*, *34*(10), 1035–1046. https://doi.org/10.1093/treephys/tpu072
Zhou, S., Yu, B., Huang, Y. F., & Wang, G. Q. (2015). Daily underlying water use efficiency for AmeriFlux sites. *Journal of Geophysical Research: Biogeosciences*, *120*, 887–902. https://doi.org/10.1002/2015JG002947